Title: Hippo and Wnt pathways are impaired in Port Wine Birthmark-derived induced pluripotent stem cells and endothelial cells

Vi Nguyen[1], Chao Gao[1], Marcelo Hochman[2,3], Jacob Kravitz[1], Elliot Chen[4,5], Harold Friedman[4,5], Camilla Wenceslau[1], Dongbao Chen[6], Yunguan Wang[7], J Stuart Nelson[8], Anil G. Jegga[7], and Wenbin Tan[1,9]

[1]Department of Cell Biology and Anatomy, School of Medicine, University of South Carolina, Columbia, South Carolina 29209, USA

[2]The Facial Surgery Center and the Hemangioma & Malformation Treatment Center, Charleston, South Carolina 29425, USA

[3]Department of Otolaryngology - Head and Neck Surgery, Medical University of South Carolina, Charleston, South Carolina 29425 USA

[4]Division of Plastic Surgery, School of Medicine, University of South Carolina, Columbia, South Carolina 29203, USA

[5]Division of Plastic Surgery, Prisma Health Medical Group, Columbia, South Carolina 29203, USA

[6]Department of Obstetrics and Gynecology, University of California, Irvine, Irvine, California 92617, USA

[7]Department of Pediatrics, Cincinnati Children Hospital, Cincinnati, Ohio 45229, USA

[8]Departments of Surgery and Biomedical Engineering, Beckman Laser Institute and Medical Clinic, University of California, Irvine, Irvine, California 92617, USA

[9]Department of Biomedical Engineering, College of Engineering and Computing, University of South Carolina, Columbia, South Carolina 29208, USA

Corresponding to:

Anil G. Jegga, Department of Pediatrics, Cincinnati Children Hospital, Cincinnati, Ohio 45229, USA; email: anil.jegga@cchmc.org

Wenbin Tan, Department of Cell Biology and Anatomy, School of Medicine, and Department of Biomedical Engineering, College of Engineering and Computing, University of South Carolina, Columbia, South Carolina, 29209, USA; email: wenbin.tan@uscmed.sc.edu

Running Title: PWB iPSCs and ECs having impaired Wnt and Hippo pathways

Funding This work was supported by grants from the National Institute of Arthritis and Musculoskeletal and Skin Diseases of the National Institutes of Health (R01AR073172 and 1R21AR083066 to WT) and Department of Defense (HT9425-23-10008 to WT).

Declaration of interests: None

Bulleted statements

What is already known about this topic?

- Port Wine Birthmark (PWB) is a congenital vascular malformation with an incident rate of 1 - 3 per 1000 births.
- PWB is resulted from developmental defects in dermal vasculature; PWB ECs have differentiational impairments.
- Pulse dye laser (PDL) is the treatment option for PWB; the efficacy has not been improved during the past three decades.

What does this study add?

- PWB iPSCs were generated through reprogramming of dermal fibroblasts and differentiated into ECs.
- PWB ECs recapulated pathological phenotypes such as forming enlarged blood vessels in vitro and in vivo.
- Hippo and Wnt pathways were impaired through PWB iPSCs to ECs during differentiation.
- Zinc-finger family was among the top changed genes in both PWB iPSCs and ECs.
- Dysregulated NF-kappa B, TNF, MAPK, and cholesterol metabolism pathways were enriched in PWB ECs.

What is the translational message?

- Hippo and Wnt pathways and ZNFs could be targeting pathways for development of paradigm-shifting therapeutics for PWB by restoring physiological differentiation of ECs.
- Targeting NF-kappa B, TNF, MAPK, and cholesterol metabolism pathways could mitigate the pathological progression of PWB.

Abstract (350)

Background: Port Wine Birthmark (PWB) is a congenital vascular malformation resulting from developmentally defective endothelial cells (ECs). Developing clinically relevant disease models is an unmet need for PWB studies.

Objective: This study aims to generate PWB-derived induced pluripotent stem cells (iPSCs) and those-iPSC-derived ECs that preserve disease-related phenotypes.

Method: PWB iPSCs were generated by reprogramming lesional dermal fibroblasts and were differentiated into ECs. Bulk RNA-seq and ATAC-seq were performed to identify enriched pathways. The functional phenotypes of iPSC-derived ECs were characterized using capillary-like structure (CLS) formation *in vitro* and Geltrex plug-in assay *in vivo*.

Result: Human PWB and normal iPSC lines were generated through reprogramming of dermal fibroblasts by introducing the "Yamanaka factors" (Oct3/4, Sox2, Klf4, c-Myc) into them; The iPSCs were differentiated into ECs. These iPSCs and their-derived ECs were validated by expression of series of stem cell and EC biomarkers, respectively. PWB EC showed impaired CLS *in vitro* with larger perimeters and thicker branches comparing with control iPSC-derived ECs. In plug-in assay, perfused human vasculature formed by PWB iPSC-derived ECs showed bigger perimeters and greater densities than those formed by control iPSC-derived ECs in SCID mice. The transcriptome analysis showed that the impaired pathways of stem cell differentiation, Hippo, Wnt, and focal adhersion persisted through PWB iPSCs to ECs during differentiation. Interactive networks showed that the Hippo and Wnt pathway-related differentially expressed genes (DEGs) significantly function in vasculature development, tube morphology, endothelium development, and EC differentiation. Members of zinc-finger (ZNF) gene family were among the top changed DEGs in both PWB iPSCs and ECs. The ZNF DEGs confer significant functions in transcriptional regulation, chromatin remodeling, protein ubiquitination, and retinol acid pathway. In addition, NF-kappa B, TNF, MAPK, and cholesterol metabolism pathways were upregulated in PWB ECs as readouts of impaired differentiation.

Conclusion: PWB iPSC-derived ECs can be served as novel and clinically relevant disease models by retaining pathological phenotypes. Our data suggests the impaired Hippo and Wnt pathways underly development of differentiation-defective ECs in PWB lesions.

Key words: Port Wine Birthmark, induced pluripotent stem cells, mesenchymal stem cells, endothelial cells, Hippo pathway, Wnt pathway, zinc-finger proteins.

Background

Congenital vascular malformations (CVMs) are a major threat to public health with a 1.5% incident rate in the general population.[1] Congenital capillary malformation (CM), a.k.a., port-wine birthmarks or stains (PWB or PWS), is the most common types of CVMs with an estimated prevalence of 0.3–0.5% per live births.[2] PWB can exist alone or coexist with many other CVMs occurring in children, such as Sturge-Weber syndrome (SWS), Parkes-Weber syndrome, and arteriovenous malformations.[3] About 25% PWB infants with forehead lesions present SWS, an ipsilateral leptomeningeal angiomatosis syndrome.[4] PWBs appear as flat red macules in childhood, which tend to progressively darken to purple. By middle age, the lesions often become raised as a result of vascular nodule development susceptible to spontaneous bleeding or hemorrhage.[2] Moreover, PWB is a disease with devastating lifelong psychological and social implications that greatly impair the quality of life of afflicted children during their development and growth.[2]

The vascular phenotypes of PWB lesions typically show the proliferation of ECs and smooth muscle cells (SMCs), the replication of basement membranes, the disruption of vascular barriers, and the progressive dilatation of vasculature.[5,6] Pathologically, PWB ECs exhibit stem-cell-like phenotypes, which are considered aberrant endothelial progenitor cells (EPCs),[5,7] leading to differentiation-defective ECs.[5] We posit that those differentiation- defective PWB ECs are responsible for these clinical manifestations. The pulsed dye laser (PDL) is the treatment of choice for PWB. Unfortunately, complete removal of PWB occurs in less than 10% of patients.[8] Second, about 20% of lesions have no response to laser treatment.[9] Between 16.3% and 50% of patients experience re-darkening of their PWB as early as 5 years after multiple PDL treatments.[9] There is no improvement in clinical outcomes using laser-based modalities for PWB treatment during the past three decades.[10] Differentiation-defective PWB ECs likely survive after laser treatments, resulting in the revascularization of lesional blood vessels after laser radiation.[5,11]

One long-term obstacle to our understanding of the pathogenesis of PWB and the therapeutic development for it has been a lack of clinically relevant cell and animal models. One strategy to overcome this barrier is to generate PWB patient-derived induced pluripotent stem cells (iPSCs). IPSCs can be reprogramed from somatic cells by introducing the “Yamanaka factors” (Oct3/4, Sox2, Klf4, c-Myc) into them, which bypasses the need for embryonic cells but retaining a patient-matching phenotype.[12] IPSCs are capable of propagating indefinitely and produce many lineages, such as EC. In this study, we successfully generated PWB patient-derived iPSCs and differentiated them into clinically relevant ECs. Those iPSC-derived ECs recapulated many

pathological phentoypes of PWB vasculatures, including formation of vasculatures with large diameters *in vitro* and *in vivo*. The impairments of Hippo and Wnt pathways could play pathogenic roles in differentiation defects of ECs, thus leadning to development of PWB vascular lesions.

Methods

Tissue preparation

The study (#1853132) was approved by the Institutional Review Board at the Prisma Health Midlands. One de-identified surgically excised PWB lesion and one de-identified surgically discarded normal skin tissue were collected for this study. The skin biopsies were cut into a size of 5 mm x 5 mm and cultured in a DMEM medium with 10% FBS for outgrowths of human dermal fibroblasts (hDFs). The hDFs were propagated and harvested for generation of iPSCs.

Generation of iPSCs and differentiation of iPSCs into ECs

The generation of iPSCs was followed using a CytoTune-iPS Sendai Reprogramming Kit (ThermoFisher, Waltham, MA). Briefly, the hDFs were cultured in a DMEM medium with 10% FBS to reach 80-90% confluence. The Sendai viral (SenV) particles were used to deliver Yamanaka factors through three vectors, e.g., polycistronic Klf4–Oct3/4–Sox2, c-Myc, and Klf4, into hDFs. The iPSC colonies were picked, isolated, and propagated under feeder-free conditions using Essential 8 Medium on a Geltrex-coated plate (ThermoFisher, Waltham, MA).

The protocol of differentiation of iPSCs into ECs was followed by several reports,[13-16] with tailored modifications. Briefly, for the induction of mesenchymal stem cells (MSCs) towards ECs, iPSCs were incubated in DMEM/F12 with human Activin A (Peprotech, 125ng/mL), B27 without insulin (1X, ThermoFisher) and geltrex (1X, ThermoFisher) on day 1. On days 2 - 4, the cells were incubated in DMEM/F12 with human BMP4 (Peprotech, 30ng/mL), human bFGF (Peprotech, 10ng/mL), human $VEGF_{165}$ (Peprotech, 50ng/mL) and geltrex (1X). The medium was changed every other day. EC induction was carried out on days 5 -7. The MSCs were incubated in StemPro complete medium with $VEGF_{165}$ (200ng/mL), 8-Br-cAMP (0.2μM), and Forskolin (2μM). The medium was changed every other day. On day 8, the ECs were passed using StemPro Accutase:Trypsin (3:1 ratio) and cultured in StemPro complete medium with VEGF (200ng/mL) and 8-Br-cAMP (0.2μM). On next day (day 9), the medium was replaced with StemPro complete medium with VEGF (200ng/mL), 8-Br-cAMP (0.2μM), and bFGF (10ng/mL). On day 11, the ECs were incubated in a regular EC growth medium (PromoCell, Heidelberg, Germany).

RNA-sequencing (RNA-seq) and data analysis

The total RNAs from iPSCs, MSCs, and ECs were extracted using a Qiagen RNA isolation kit. The ribosomal RNAs were depleted using a Qiagen rRNA HMR kit. RNA-seq libraries were constructed using a Qiagen Standard RNA Library kit followed by the manufacture manual. For ATAC-seq, the nuclei iPSCs, MSCs, and ECs were extracted. The insertion size of the libraries was determined using an Agilent 2100 Bioanalyzer system (Santa Clara, CA, USA). Library quantification was carried out using a NGS library quantification kit from Takara Bio. Paired-end sequencing was performed on a NovaSeq 6000 system (Illumina, San Diego, CA, USA) for 25-50 M reads per library. For RNA-seq, the raw reads were aligned and mapped to human reference genome using STAR.[17] Validation and quantification of RNA transcripts were performed using FeatureCounts.[18] Biostatistical analysis for differentially expressed genes (DEGs) among groups and data graphic generation were carried out in the Rstudio package (https://www.rstudio.com/). False discovery rate (FDR) < 0.01 was considered significant. Gene ontology (GO) for enrichment analysis on gene sets and Kyoto Encyclopedia of Genes and Genomes (KEGG) for enrichment pathway analysis were performed based on DEGs.

Using gene ontology and various pathway database gene annotations, we compiled a list of known Wnt and Hippo signaling pathway genes. In addition, for Hippo signaling, we used the Hippo pathway interaction proteome which included 343 new protein interactions for human hippo components (https://pubmed.ncbi.nlm.nih.gov/24366813/). For Zinc finger gene set compilation, we used gene families from the HUGO (June 2027; HGNC Database, HUGO Gene Nomenclature Committee (HGNC), European Molecular Biology Laboratory, European Bioinformatics Institute (EMBL-EBI), Wellcome Genome Campus, Hinxton, Cambridge CB10 1SD, United Kingdom www.genenames.org). These compiled lists of genes (Supplementary File 1) were used to obtain the EC, iPSC, MSC DEGs that were associated with Hippo or Wnt signaling pathways or were known to encode Zinc-finger proteins (ZNFs). Details of the intersections are included in the Supplementary File.

Venn diagram to illustrate the overlap between DEG from iPSC, MSC, EC and compiled sets of known Hippo or Wnt signaling pathway genes or ZNFs were generated using Venny (https://bioinfogp.cnb.csic.es/tools/venny/index.html). Heatmap representation of the intersecting genes were generated using the Morpheus application (https://software.broadinstitute.org/morpheus). For functional characterization of the intersecting gene sets, we used the ToppFun application of the ToppGene Suite.[19] All networks were generated using the Cytoscape application.[20]

Geltrex *in vitro* capillary-like structure (CLS) formation

The CLS formation of angiogenesis from ECs can be modeled *in vitro* by a Geltrex or Matrigel-based tube formation assay.[21,22] ECs plated on Geltrex/Matrigel at low densities form a network of branching structures which can be photographed and quantified by measuring the length, perimeter or area of CLS.[21,22] CLS formation was performed in 24-well plates. Briefly, Geltrex (ThermoFisher, Waltham, MA) (200 µl per well) was added into a 24-well plate and incubated at 37ºC for 30 minutes. ECs (n=4 for each cell model) were trypsinized and resuspended in EC basal medium without supplements. Each type of cells ($4.5x10^4$ in 200 µl) were then added into each well and incubated at 37ºC with 5% CO2 for 12-16 hrs to form CLS. The cells were fixed by 4% buffered formalin at the end of experiments. The images were acquired using an EVOS system (ThermoFisher, Waltham, MA). The CLS wall thickness, perimeter and area of branching point were outlined from the acquired images and directly measured by using the ImageJ software.

In vivo xenograft assay in severe combined immune deficient (SCID) mice

The experimental procedures have been approved in an animal protocol (# 2581-101681-020822, approval date: 07/29/2022; Dr. Tan) according to the University of South Carolina institutional animal care and use committee (IACUC). We implanted iPSC-derived normal and PWB ECs and mesenchymal stem cells (MSCs) with Geltrex into the subcutaneous layer of the skin of SCID mice using a protocol courtesy of Dr. Bischoff at the Boston Children Hospital, Harvard University.[23,24] SCID mice (Nude NIH-III) from Charles River were used. For the transdermal xenografting, each of the normal or PWB EC/MSC (2×10^6 cells with a ratio of EC:MSC as 2:3) will be mixed with Geltrex in a total volume of 200 µl per injection. A negative control with Geltrex only without cells will be included. Each animal will be assigned three distinct injection sites in the abdominal flanks. A pair of normal and PWB EC/MSC/Matrigel mixture and the Geltrex only negative control will be injected into one of three sites in a SCID mouse, respectively. This will allow for side-by-side comparison to minimize inter-animal variables and reduce animal number usage. The animals were sanctified at the day 10th post-injection to examine the formation and remodeling of PWB-like dermal vasculatures *in vivo*. The plug-ins were removed, fixed, embedded, and sectioned.

Immunofluorescent (IF) staining and immunohistochemistry (IHC)

The paraffin sections of plug-ins were deparaffinized according to routine procedures. The antigen retrieval was performed in 10 mM sodium citrate buffer (pH 6.0) at 97ºC for 2-4 hrs. The sections were then incubated in a humidified chamber for overnight at 4ºC with a biotinylated anti-human Ulex europaeus agglutinin I (UEA1) (Vector Laboratories, Newark, CA; #B-1065-2, 1:100 dilution).

An indirect biotin avidin diaminobenzidine (DAB) system (Dako, Glostrup, Denmark) was used for detection.

The iPSCs or ECs were grown in Geltrex-coated or fibronectin-coated coverslips and fixed using 4% buffered paraformaldehyde. The cells were blocked using 5% normal donkey serum, followed by overnight incubation with the following primary antibodies at 4ºC (1:100 dilution): anti-Tra1-60 (Abcam, #ab16288), anti-Nanog (Abcam, #ab21624), anti-Sox2 (Abcam, #ab79351), anti-Oct4 (Abcam, #ab19857), anti-CD31 (Sigma-Millipore, #ZRB1216), and anti-human CD144/VE-Cadherin (ThermoFisher, #14-1449-82). Alexa - 488 or - 555 fluorescent-conjugated anti-rabbit or mouse secondary antibodies (ThermoFisher) were incubated with sections (1:200 dilution) for 1 hr at room temperature after the primary antibodies' reaction. Negative controls were performed without primary antibodies. Images acquired using Leica Stellaris 5 DMS CS confocal microscope.

Statistics. The paired samples t-tests were performed to evaluate the statistical differences of morphological parameters among vasculature, and differences between PWB and normal control data sets. Data presented as "mean ± S.D." and $p < 0.05$ were considered significant.

Results

Six to eight days after the delivery of Yamanaka factors into hDFs, the formation of iPSC colonization was observed (Fig 1A). The iPSC colonies were confirmed using an alkaline phosphate live staining (Fig 1B). The initial iPSC colonies were picked, isolated, and propagated. Some colonies were prone to differentiate and difficult to maintain pluripotency status during screening and propagation (data not shown). Those colonies were thus discarded. Two iPSC lines from a human PWB lesion (#4221_3 and #4221_6) and three lines from normal skin (#52521_4, #52521_8 and #52521_9) were successfully expanded and maintained for more than 50 passages, respectively. These cells were further verified to express iPSC biomarkers of Tra1-60, Nanog, Oct4, and Sox2 using IF staining (Fig 1C-F). In the following EC differentiation and functional characterizations, we mainly focused on PWB iPSC 4221_3 and control iPSC 52521_9 lines.

Our tailored EC differentiation protocol was outlined in Fig 2A. The differentiation of PWB iPSCs into MSCs was induced on the second day (Fig 2B). Fully differentiated monolayer ECs from PWB iPSCs on the eighth day after induction. Approximately 95% purity (based on CD31+ cell profile in flow cytometry, data not shown) of EC population were achieved from MSCs. The molecular phenotypes of iPSC-dervied ECs were verified using IF staining with antibobodies recognizing specific biomarkers CD31 and CD144 (Fig 2C,D).

The CLS formation has been used to assess morphological differentiations among a variety of ECs.[25] In effort to examine whether PWB ECs could recapitulate pathological phenotypes of PWB vasculature, we first performed CLS formation on Geltrex *in vitro* to characterize the morphologies of vasculatures formed by PWB iPSC-derived ECs (Fig 2E-H). The CLS formed by PWB EC_4221 in Geltrex *in vitro* had larger perimeters and greater thickness in branches than those formed by normal EC_52521 (Fig 2E-H). Second, we implanted iPSC-derived normal and PWB ECs and MSCs with Geltrex into the subcutaneous layer of the skin of SCID mice. Perfused PWB or normal vasculatures were formed in dermal implants ten days after xenografting (Fig. 3A-B), which comprised human ECs recognized by anti-human UEA1 antibody (Fig. 3C-D). The vasculature formed by PWB ECs had larger perimeters and higher density than those formed by normal ECs (Fig3. E-G); size distribution showed that the total percentage of perfused large vessels (perimeters > 100 μm) formed by PWB iPSC-derived ECs was significantly higher than those formed by the control iPSC-derived ECs (41.2% vs 16.5%). This was consistent with data from patients' lesions in our previous report[5] as well as an xenografted animal model by Dr. Bischoff group.[23]

Next, we compared the transcriptomes of PWB iPSCs, MSCs, and ECs with theor control couterparts using RNA-seq. PWB iPSC 4221 lines showed 1375 upregulated DEGs and 1717 downregulated DEGs as compared to control iPSC 52521 lines (FDR<0.05) (Fig 4). PWB MSC 4221 lines showed 644 upregulated DEGs and 744 downregulated DEGs (FDR<0.05) (Fig 5). PWB EC 4221 lines showed 655 upregulated DEGs and 371 downregulated DEGs (FDR<0.05) (Fig 6). DEGs related to Hippo and Wnt pathways were consistantly present through iPSC, MSCs to ECs, as the main significantly enriched pathways during the entire course of differentiation (Fig 4-6). Members of ZNF gene family were among the top changed DEGs in both PWB iPSCs and ECs (Fig 7). In PWB iPSCs, there were 108 downregulated DEGs and 93 upregulated DEGs related to ZNF family (Fig 7).

Interactive networks showed that the DEGs in Hippo and Wnt pathways confer significant functions in vasculature development, tube morphology, endothelium development, and EC differentiation (Fig 8A,B). The ZNF DEGs showed significant functions in transcriptional regulation, chromatin remodeling, protein ubiquitination, and retinol acid pathway (Fig 8C). The KEGG pathway analysis showed the significantly upregulated pathways in PWB iPSCs including calcium signaling, gap junction, fatty acid biosynthesis, and vascular smooth muscle contraction (Fig 8D). Upregulations of TNF, NF-kappa B, MAPK, and cholesterol metabolism were found in PWB ECs only, suggesting that these pathways were likely secondary pathologies, a result from differention defects during vascular development (Fig 8D). The overlapped downregulated pathways in PWB iPSCs and ECs included Hippo, Wnt, regulating pluripotency of stem cells, TGF-beta, axon guidance, and focal adhesion, suggesting their potential roles in both diease development and progression (Fig 8E). Tight junction and cell adhesion were among the significantly downregulated pathways in PWB iPSCs (Fig 8E). GO enrichment analysis showed the top dysregulated biological processes included regulation of developmental process, tissue/blood vessel differentiation and development, cell differentiation, tube morphogenesis, cell adhesion in PWB iPSCs, MSCs, and ECs (Supplementary File 2).

Discussion

In this study, we have successfully generated PWB patient-derived iPSCs and differentiated them into ECs. These cells recapitulate many vascular phenotypes from the donor lesions, which can be used as a novel disease modeling for PWB. The dysregulated pathways such as Hippo, Wnt, regulating pluripotency of stem cells persist through PWB iPSCs to ECs during differentiation process. This data suggests their causal roles in both diease development and progression. Upregulations of TNF, NF-kappa B, MAPK, and cholesterol metabolism are present in PWB ECs but not evident in iPSCs. It suggests that impairments of these pathways are downdream results from differention defects during vascular development. Our data also suggests that impaired Hippo and Wnt pathways can be drugable targets for therapeutic development for PWB treatment.

The unlimited self-renewal, pluripotency, and all-cell-type-differentiation capability have made iPSC mark its revolutionizing way in disease modeling, drug screening, tissue engineering, precision medicine, and regenerative therapeutics since the first day of its birth in 2006.[12,26] Particularly, genetic aberrations can be inherited by iPSCs from the somatic cells and can be passed through to generations of iPSCs and their-differentiated daughter cells, thus retaining and exhibiting the disease phenotypes from the donor tissues. This makes iPSC and their-derived vascular cells be attractive cell models for the study of PWB. There are many reprogramming strategies. The integrative transgene delivery methods using lenti- or retroviral systems usually cause safety concerns such as mutagenicity for the cell-based therapy.[26] In this study, we used a non-integrating SenV system for hDF reprogramming, a strategy allowing long-last transgenic expression of the “Yamanaka factors” and leading to considerable efficiency.[27] The trace of SenV components could last for ten passages.[28] We used iPSC lines after 30-50 passages for differentiation and functional characterization. Therefore, the effects of SenV should be minimal in our cell models. In this study, the generated PWB iPSCs and iPSC-derived ECs retain many clinically relevant vascular phenotypes thus data from them are readily translational. Therefore, these cells are particularly valuable as cell models in the field of CVMs, circumventing the hurdle of disease model absence.

Studies have shown that sporadic somatic mutations of the guanine nucleotide-binding protein, G alpha subunit q (GNAQ) (R183Q), and phosphatidylinositol 3-kinase (PI3K) are linked to the vascular phenotypes of PWB[29-31]. We, and Cuoto et al., further showed that the GNAQ (R183Q) is present in ECs or blood vessels,[11,32] connective tissues, hair follicles and glands in PWB lesions, suggesting that pluripotent cells with GNAQ (R183Q) give rise to multi-lineages in PWB.[11] An excellent study has shown that ECs with GNAQ (R183Q) can cause active phospholipase C

(PLC) β3 signaling, increase angiopoietin-2 (ANGPT2), and produce enlarged capillary-like vessels.[23] Despite these findings, our view of the role of GNAQ (R183Q) in PWB remains incomplete. (1) In the skin lesions, PWB vasculatures show GNAQ (R183Q) allelic frequencies ranging from 3 to 12 percent.[11] It has been unclear whether and how 3-12% GNAQ (R183Q) ECs are sufficient to cause a full spectrum of skin pathological phenotypes including progressive vascular dilation, SMC proliferation, axon defects, and disorganized collagen fibers. (2) The PWB patient-derived iPSC lines in this study do not harbor the GNAQ (R183Q) mutation (data not shown) but present many clinically relevant vascular phenotypes. These observations suggest that there is a GNAQ (R183Q)-independent mechanism associated with the development of PWB vascular phenotypes. (3) It is yet to be determined whether impaired Hippo/Wnt pathways and GNAQ (R183Q) could act synergistically and accelerate the pathological process of PWB.

PWB is a reslult from developmental defects of vasculature during embryoic stages. This is supported by the evidnce that PWB ECs exhibit stem-cell-like phenotypes.[5,7] There is a thirst for knowledge between the developmental defects of PWB ECs and underlying mechanisms. The Hippo pathway plays a fundamental role in controlling organ size, stem cell proliferation, and tissue repair and regeneration.[33,34] The Wnt pathway conveys crucial signaling that regulates cell fate, migration, polarity, and organogenesis.[35,36] The crosstalk between these two signalosomes coordinately executes their functions during development.[37,38] As the facts of developmental vascular defects and soft tissue outgrowth in PWB, it is reasonable to posit the critical roles of impaired Hippo and Wnt pathways in the developmental defects and progression of vascular phenotypes in PWB lesions. Indeed, the impairments of Hippo and Wnt pathways have been found through a whole transcriptome atlas analysis of individual lesional vasculature on PWB formalin-fixed paraffin-embedded (FFPE) sections using a GeoMx digital spatial profiler (Nguyen, Wang, Jegga and Tan, personal communications). This data demonstrates that the impaired Hippo and Wnt pathways in PWB iPSCs could be inherited from PWB lesional tissues and passed into MSCs and ECs during differentiation. There are two possible underlying mechanisms: (1) PWB iPSCs thoroughly replicate the genome of lesional hDFs, such as processing related genetic abnormalities from lesional hDFs, thus preserving impaired Hippo and Wnt pathways and recapitulated into their differentiated ECs; and (2) PWB iPSCs retain an 'epigenetic memory' of lesional hDFs, through which disease-related DNA methylation signatures are preserved from the original somatic cells.[39] This could make PWB iPSCs be prone to lineage differentiation propensity of donor ECs, thus matching disease associated phenotypes.

Members of ZNFs were among the most changed DEGs in PWB iPSCs, MSCs, and ECs. The zinc-finger domains of ZNFs confer interactions with DNA, RNA, and proteins, involving many

cellular processes such as transcriptional regulation, chromatin remodeling, ubiquitin-mediated proteasome, retinol acid signaling.[40] Transcriptional factors are determining factors for cell fate and lineage decision-making during development. As a major group of transcriptional modulators, ZNFs may play an important role in regulating Hippo and Wnt pathways in PWB. For example, both ZNF E-box-binding homebox (ZEB) 1 and 2 were upregulated in PWB iPSCs. ZEBs function as a transcriptional repressor for epithelial genes to maintain an undifferentiated phenotype during epithelial-mesenchymal transition (EMT).[41] TGF-β responsive genes and cell adhesion and junction genes are the transcriptional targets of ZEBs.[41] Evedence also has shown the direct transcriptional regulation of ZNFs on Hippo pahtways. For example, ZEB1 can directly interact with YAP, switching ZEB1 from a repressor to a transcriptional activator to cause cancer-promoting effects.[42] This evidence suggests the potential role of ZNFs in disease development of PWB, but the detailed mechanisms are yet to be determined in future studies.

In conclusion, PWB iPSCs and their-derived ECs generated in this study retain pathological vascular phenotypes and can be served as clinically relevant models. Our data suggests the impaired Hippo and Wnt pathways underly development of differentiation-defective ECs in PWB lesions.

Figure legend:

Figure 1: Generation of normal skin and PWB-derived iPSCs. (A) an iPSC colony raised from hDF after reprogramming. (B) a typical morphology of a control iPSC colony, Ctl_iPSC_52521_8. (C) PWB iPSC 4221_3 under bright flied. (D) AP staining on the same iPSC colony. (E) and (F) control and PWB iPSC colonies were expression stem cell biomarkers Nanog and Tra1-60. (G) and (H) stem cell biomarkers Sox2 and Oct4 were used to verify the control and PWB iPSC cells. DAPI staining was used for nuclei.

Figure 2: Differentiation of iPSCs into ECs and functional charaterizations of PWB iPSC-derived ECs. (A) A flowchart of iPSC differentiation protocol. (B) The morphological changes during PWB iPSC differentiation through MSCs into ECs. MSCs were induced from iPSCs on day 2-4 with a course to EC lineage. The EC induction was performed through day 5 to day 12. Fully differentiated monolayer ECs from PWB IPSCs were observed on the eighth day. (C) and (D) control and PWB iPSC-derived ECs were expressed EC membrane biomarkers CD31 (red) and CD144 (green). Nuclei was stained by DAPI. (E) and (F) control EC_52521_9 and PWB EC_4221_3 formed CLS on Geltrex. (G) and (H) PWB EC_4221_3 showed impaired CLS *in vitro* with larger perimeters (G) (p=5.09x10^{-32}) and thicker branches (H) (p=1.27x10^{-41}) comparing with control EC_52521_9. Whiskers: mean±S.D.; Diamond box: interquartile range (IQR); Dotted curve: data distribution. A Mann-Whitney U test was used.

Figure 3: PWB iPSC-derived ECs formed phologically phenoyptic blood vessels in vivo. (A) and (B) Formation of perfused human vasculature 10 days after intradermal xenograft of control (A) and PWB (B) ECs with the corresponding MSCs into SCID mice. Arrows: perfused blood vessels in xenografts (H&E staining). (C) and (D) Perfused vasculature comprising human ECs was confirmed using immunohistochemsitry (IHC) by an anti-human UEA1 antibody in both control and PWB ECs. (E) Perimeter distrubtion of xenografted vasculature formed by PWB ECs compared to control vasculature. Pink dashed rectangle: the total percentage (41.2%) of perfused vessels formed by PWB iPSC-derived ECs as compared with 16.5% of perfused vessels formed by control iPSC-derived ECs with perimeters over 100 μm. (F and G) Perfused vasculature formed by PWB iPSC-derived ECs showed (F) bigger perimeters (p=3.68x10^{-6}) and (G) greater densities (per mm^2) (p=8.72x10^{-7}) than those formed by normal ECs. Whiskers: mean±S.D.; Diamond boxes: IQR; Dotted curves: data distribution. A Mann-Whitney U test was used.

Figure 4: RNA-seq analysis and DEG enrichemnt in Hippo and Wnt pathways in PWB iPSCs. (A) Volcano plot showing the DEGs in PWB iPSCs as compared to control iPSCs. (B) Heatmap showing the total DEGs in PWB iPSCs vs control iPSCs. (C) Heatmap presenting DEGs in Hippo pathway. (D) Heatmap showing DEGs in Wnt pathway. (E) Venn diagram to illustrate

up- and down- regulated DEGs in Hippo and Wnt pathways in PWB iPSCs as compared to control iPSCs.

Figure 5: RNA-seq analysis and DEG enrichemnt in Hippo and Wnt pathways in PWB iPSC-derived MSCs. (A) Volcano plot showing the DEGs in PWB iPSC-derived MSCs as compared to control iPSC-derived MSCs. (B) Heatmap showing the total DEGs in PWB iPSC-derived MSCs vs control iPSC-derived MSCs. (C) Heatmap presenting DEGs in Hippo pathway. (D) Heatmap showing DEGs in Wnt pathway. (E) Venn diagram to illustrate up- and down- regulated DEGs in Hippo and Wnt pathways in PWB iPSC-derived MSCs as compared to control iPSC-derived MSCs.

Figure 6: RNA-seq analysis and DEG enrichemnt in Hippo and Wnt pathways in PWB iPSC-derived ECs. (A) Volcano plot showing the DEGs in PWB iPSC-derived ECs as compared to control iPSC-derived ECs. (B) Heatmap showing the total DEGs in PWB iPSC-derived ECs vs control iPSC-derived ECs. (C) Heatmap presenting DEGs in Hippo pathway. (D) Heatmap showing DEGs in Wnt pathway. (E) Venn diagram to illustrate up- and down- regulated DEGs in Hippo and Wnt pathways in PWB iPSC-derived ECs as compared to control iPSC-derived ECs.

Figure 7: ZNF family is among the top changed DEGs. (A), (B) and (C) Heatmap presenting DEGs in ZNFs in PWB iPSCs (A), MSCs (B), and ECs (C) as compared with their control counterparts. (D) Venn diagram to illustrate up- and down- regulated DEGs in ZNFs in PWB iPSCs, MSCs, and ECs as compared with their control counterparts.

Figure 8: Functional interative networks of DEGs in Hippo and Wnt pathways and ZNF family. (A) Functional interactive network of Hippo- and Wnt-related DEGs in PWB vasculature showing significant enrichment (FDR<0.05) for tube morphogenesis, endothelium and vasculature development, and EC differentiation. (B) Functional characterization of the intersecting DEGs in Hippo and Wnt pathways in affected biological processes. (C) Functional modulations of biological pathways by the DEGs in ZNFs. (D) and (E) KEGG enrichment analysis showing significantly upregulated (D) and downregulated (E) pathways related to vascular differentiation and development in PWB iPSCs and ECs.

Acknowledgement for the DoD award HT9425-23-10008

i. "The U.S. Army Medical Research Acquisition Activity, 820 Chandler Street, Fort Detrick MD 21702-5014 is the awarding and administering acquisition office." and;

ii. "This work was supported by The Assistant Secretary of Defense for Health Affairs endorsed by the Department of Defense, in the amount of $297,956.00, through the Peer Reviewed Medical Research Program under Award Number (HT9425-23-10008). Opinions, interpretations, conclusions, and recommendations contained herein are those of the author(s) and are not necessarily endorsed by the Department of Defense."

i. "In conducting research using animals, the investigator(s) adhere(s) to the laws of the United States and regulations of the Department of Agriculture."

i. "In the conduct of research utilizing recombinant DNA, the investigator(s) adhered to NIH Guidelines for research involving recombinant DNA molecules."

ii. "In the conduct of research involving hazardous organisms or toxins, the investigator(s) adhered to the CDC-NIH Guide for Biosafety in Microbiological and Biomedical Laboratories."

Database deposition

The raw data (reads in fastq files) and processed files (aligned bam files) of RNA-seq are deposited into NIH SRA (Sequence Read Archive). The transcriptome data are deposited into GEO (Gene Expression Omnibus). Data are available to the public.

References

1 Eifert, S., Villavicencio, J. L., Kao, T. C., Taute, B. M. & Rich, N. M. Prevalence of deep venous anomalies in congenital vascular malformations of venous predominance. *J. Vasc. Surg.* 2000; **31**: 462-471.

2 Lever, W. F. & Schaumburg-Lever, G. *Histopathology of the Skin*. 7th edn, (J.B. Lippincott Co., 1990).

3 ISSVA. ISSVA Classification of Vascular Anomalies. *International Society for the Study of Vascular Anomalies.* 2014; **issva.org/classification**.

4 Waelchli, R. *et al.* New vascular classification of port-wine stains: improving prediction of Sturge-Weber risk. *Br. J. Dermatol.* 2014; **171**: 861-867.

5 Tan, W. *et al.* Coexistence of EphB1 and EphrinB2 in Port Wine Stain Endothelial Progenitor Cells Contributes to Clinicopathological Vasculature Dilatation. *Br. J. Dermatol.* 2017; **177**: 1601-1611.

6 Tan, W. *et al.* Pathological Alterations Involve the Entire Skin Physiological Milieu in Infantile and Early Childhood Port Wine Stain. *Br. J. Dermatol.* 2016; **177**: 293-296.

7 Williams, J. *et al.* Embryonic Stem Cell-like Population in Hypertrophic Port-wine Stain. *Journal of Vascular Anomalies* 2021; **2**.

8 Nelson, J. S., Jia, W., Phung, T. L. & Mihm, M. C., Jr. Observations on enhanced port wine stain blanching induced by combined pulsed dye laser and rapamycin administration. *Lasers Surg. Med.* 2011; **43**: 939-942.

9 Savas, J. A., Ledon, J. A., Franca, K., Chacon, A. & Nouri, K. Pulsed dye laser-resistant port-wine stains: mechanisms of resistance and implications for treatment. *Br. J. Dermatol.* 2013; **168**: 941-953.

10 van Raath, M. I. *et al.* Port wine stain treatment outcomes have not improved over the past three decades. *J. Eur. Acad. Dermatol. Venereol.* 2019; **33**: 1369-1377.

11 Tan, W. *et al.* The somatic GNAQ mutation (R183Q) is primarily located in Port Wine Stain blood vessels. *J. Am. Acad. Dermatol.* 2016; **74**: 380-383.

12 Takahashi, K. & Yamanaka, S. Induction of pluripotent stem cells from mouse embryonic and adult fibroblast cultures by defined factors. *Cell* 2006; **126**: 663-676.

13 Ikuno, T. *et al.* Efficient and robust differentiation of endothelial cells from human induced pluripotent stem cells via lineage control with VEGF and cyclic AMP. *PLoS One* 2017; **12**: e0173271.

14 Williams, I. M. & Wu, J. C. Generation of Endothelial Cells From Human Pluripotent Stem Cells. *Arterioscler. Thromb. Vasc. Biol.* 2019; **39**: 1317-1329.

15 Patsch, C. *et al.* Generation of vascular endothelial and smooth muscle cells from human pluripotent stem cells. *Nat. Cell Biol.* 2015; **17**: 994-1003.

16 Rufaihah, A. J. *et al.* Human induced pluripotent stem cell-derived endothelial cells exhibit functional heterogeneity. *Am J Transl Res* 2013; **5**: 21-35.

17 Dobin, A. *et al.* STAR: ultrafast universal RNA-seq aligner. *Bioinformatics* 2013; **29**: 15-21.

18 Liao, Y., Smyth, G. K. & Shi, W. featureCounts: an efficient general purpose program for assigning sequence reads to genomic features. *Bioinformatics* 2014; **30**: 923-930.

19 Chen, J., Bardes, E. E., Aronow, B. J. & Jegga, A. G. ToppGene Suite for gene list enrichment analysis and candidate gene prioritization. *Nucleic Acids Res.* 2009; **37**: W305-311.

20 Shannon, P. *et al.* Cytoscape: a software environment for integrated models of biomolecular interaction networks. *Genome Res.* 2003; **13**: 2498-2504.

21 Goodwin, A. M. In vitro assays of angiogenesis for assessment of angiogenic and anti-angiogenic agents. *Microvasc. Res.* 2007; **74**: 172-183.

22 Kubota, Y., Kleinman, H. K., Martin, G. R. & Lawley, T. J. Role of laminin and basement membrane in the morphological differentiation of human endothelial cells into capillary-like structures. *J. Cell Biol.* 1988; **107**: 1589-1598.
23 Huang, L. *et al.* Endothelial GNAQ p.R183Q Increases ANGPT2 (Angiopoietin-2) and Drives Formation of Enlarged Blood Vessels. *Arterioscler. Thromb. Vasc. Biol.* 2022; **42**: e27-e43.
24 Melero-Martin, J. M. *et al.* Engineering robust and functional vascular networks in vivo with human adult and cord blood-derived progenitor cells. *Circ. Res.* 2008; **103**: 194-202.
25 Arnaoutova, I., George, J., Kleinman, H. K. & Benton, G. The endothelial cell tube formation assay on basement membrane turns 20: state of the science and the art. *Angiogenesis* 2009; **12**: 267-274.
26 Poetsch, M. S., Strano, A. & Guan, K. Human Induced Pluripotent Stem Cells: From Cell Origin, Genomic Stability, and Epigenetic Memory to Translational Medicine. *Stem Cells* 2022; **40**: 546-555.
27 Giallongo, S. *et al.* Redox and Epigenetics in Human Pluripotent Stem Cells Differentiation. *Antioxid. Redox Signal.* 2021; **34**: 335-349.
28 Trokovic, R. *et al.* Advanced feeder-free generation of induced pluripotent stem cells directly from blood cells. *Stem Cells Transl Med* 2014; **3**: 1402-1409.
29 Lian, C. G. *et al.* Novel Genetic Mutations in a Sporadic Port-Wine Stain. *JAMA Dermatol* 2014; **150**: 1336-1340.
30 Shirley, M. D. *et al.* Sturge-Weber Syndrome and Port-Wine Stains Caused by Somatic Mutation in GNAQ. *N. Engl. J. Med.* 2013; **368**: 1971-1979.
31 Luks, V. L. *et al.* Lymphatic and other vascular malformative/overgrowth disorders are caused by somatic mutations in PIK3CA. *J. Pediatr.* 2015; **166**: 1048-1054 e1041-1045.
32 Couto, J. A. *et al.* Endothelial Cells from Capillary Malformations Are Enriched for Somatic GNAQ Mutations. *Plast. Reconstr. Surg.* 2016; **137**: 77e-82e.
33 Halder, G. & Johnson, R. L. Hippo signaling: growth control and beyond. *Development* 2011; **138**: 9-22.
34 Johnson, R. & Halder, G. The two faces of Hippo: targeting the Hippo pathway for regenerative medicine and cancer treatment. *Nat. Rev. Drug Discov.* 2014; **13**: 63-79.
35 Steinhart, Z. & Angers, S. Wnt signaling in development and tissue homeostasis. *Development* 2018; **145**.
36 Nusse, R. & Clevers, H. Wnt/beta-Catenin Signaling, Disease, and Emerging Therapeutic Modalities. *Cell* 2017; **169**: 985-999.
37 Li, N., Lu, N. & Xie, C. The Hippo and Wnt signalling pathways: crosstalk during neoplastic progression in gastrointestinal tissue. *FEBS J.* 2019; **286**: 3745-3756.
38 Azzolin, L. *et al.* YAP/TAZ incorporation in the beta-catenin destruction complex orchestrates the Wnt response. *Cell* 2014; **158**: 157-170.
39 Kim, K. *et al.* Epigenetic memory in induced pluripotent stem cells. *Nature* 2010; **467**: 285-290.
40 Cassandri, M. *et al.* Zinc-finger proteins in health and disease. *Cell death discovery* 2017; **3**: 17071.
41 Vandewalle, C., Van Roy, F. & Berx, G. The role of the ZEB family of transcription factors in development and disease. *Cellular and molecular life sciences : CMLS* 2009; **66**: 773-787.
42 Lehmann, W. *et al.* ZEB1 turns into a transcriptional activator by interacting with YAP1 in aggressive cancer types. *Nature communications* 2016; **7**: 10498.

Fig 1

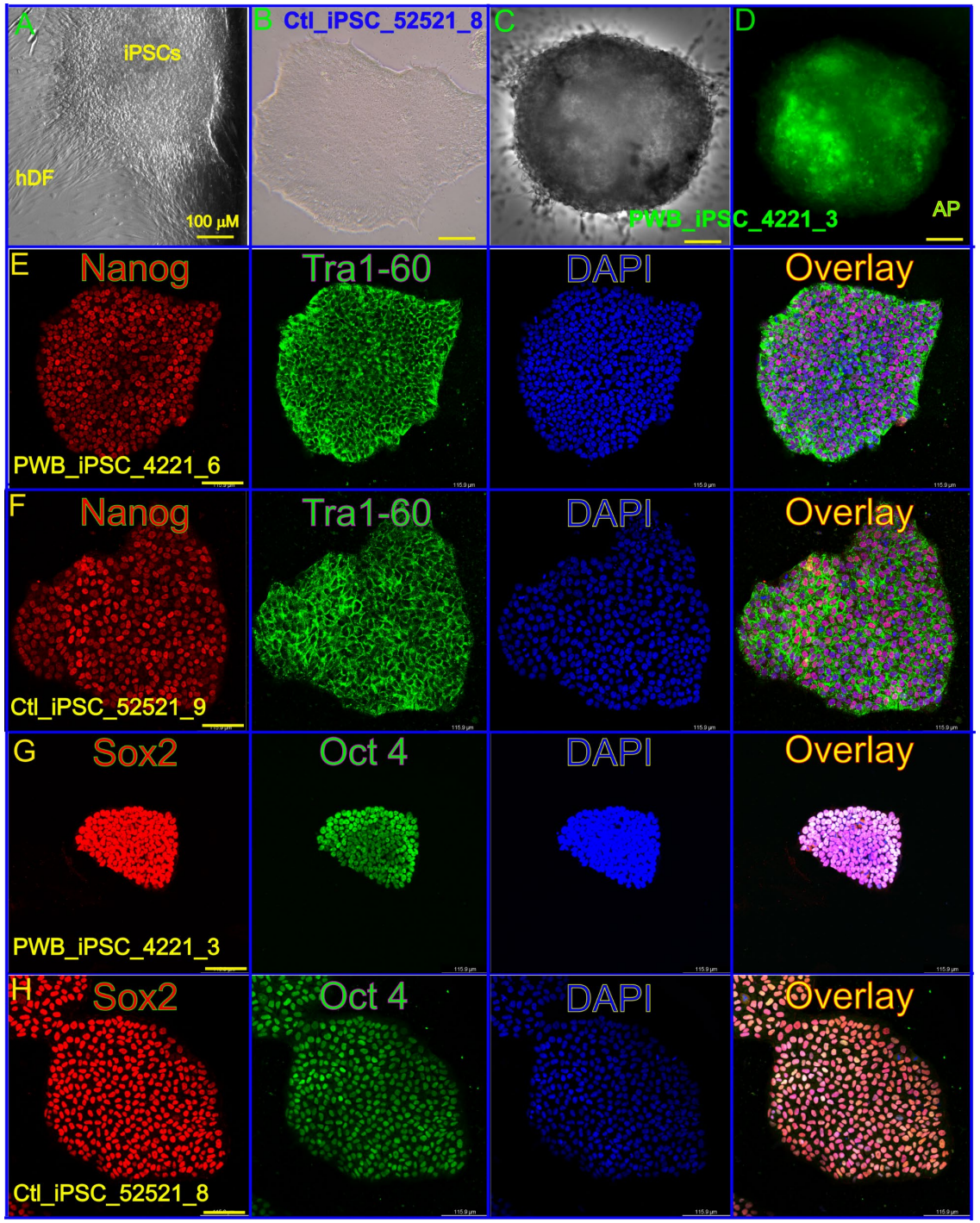
A
iPSCs
hDF
100 µM
B Ctl_iPSC_52521_8
C
PWB_iPSC_4221_3
D
AP
E
Nanog
Tra1-60
DAPI
Overlay
PWB_iPSC_4221_6
F
Nanog
Tra1-60
DAPI
Overlay
Ctl_iPSC_52521_9
G
Sox2
Oct 4
DAPI
Overlay
PWB_iPSC_4221_3
H
Sox2
Oct 4
DAPI
Overlay
Ctl_iPSC_52521_8

Fig 2

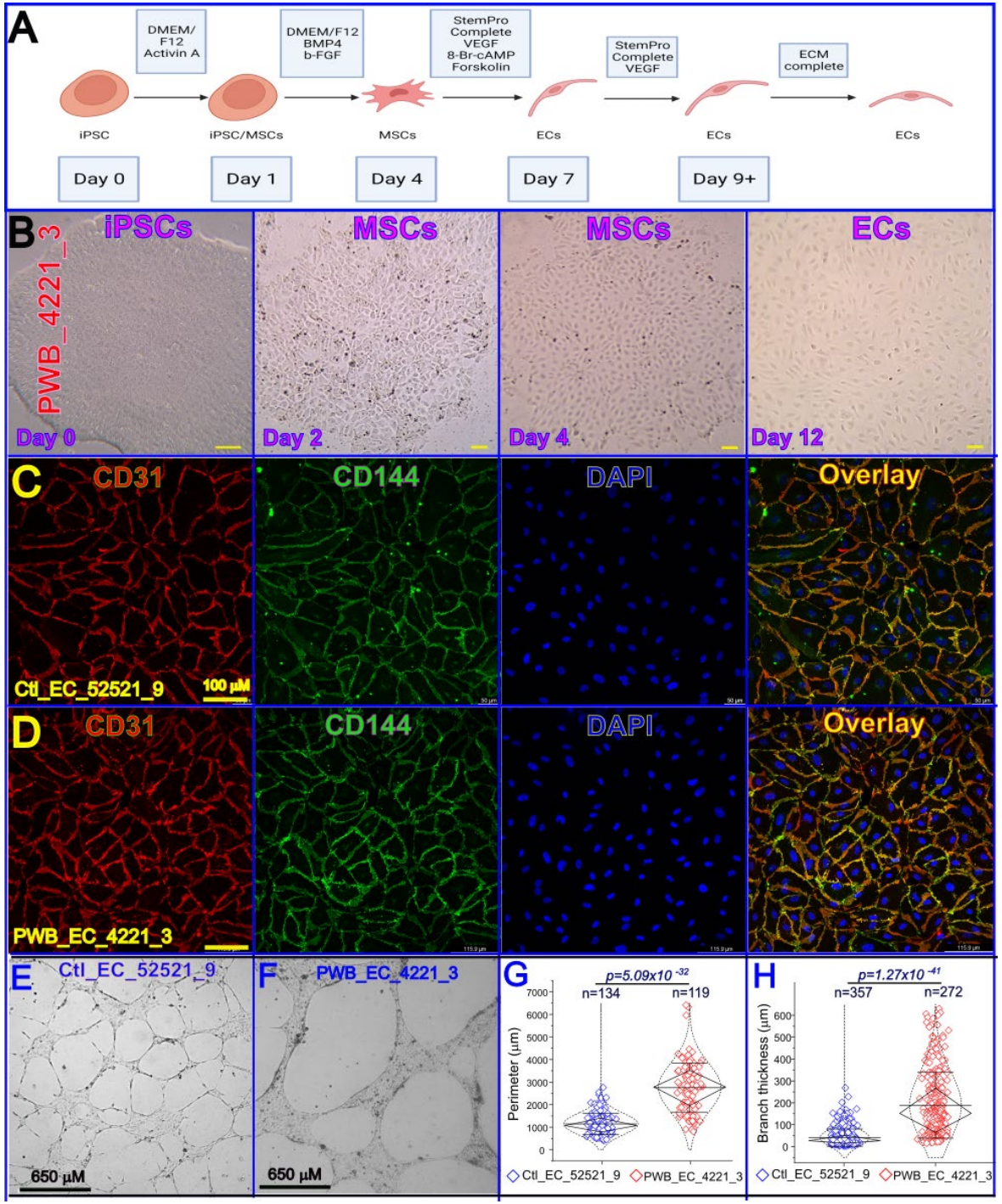
A
DMEM/ F12 Activin A
DMEM/F12 BMP4 b-FGF
StemPro Complete VEGF 8-Br-cAMP Forskolin
StemPro Complete VEGF
ECM complete
iPSC
iPSC/MSCs
MSCs
ECs
ECs
ECs
Day 0
Day 1
Day 4
Day 7
Day 9+
B
PWB_4221_3
iPSCs
MSCs
MSCs
ECs
Day 0
Day 2
Day 4
Day 12
C
CD31
CD144
DAPI
Overlay
Ctl_EC_52521_9
100 µM
D
CD31
CD144
DAPI
Overlay
PWB_EC_4221_3
E
Ctl_EC_52521_9
650 µM
F
PWB_EC_4221_3
650 µM
G
p=5.09x10 -32
n=134
n=119
Perimeter (µm)
Ctl_EC_52521_9
PWB_EC_4221_3
H
p=1.27x10 -41
n=357
n=272
Branch thickness (µm)
Ctl_EC_52521_9
PWB_EC_4221_3

Fig 3

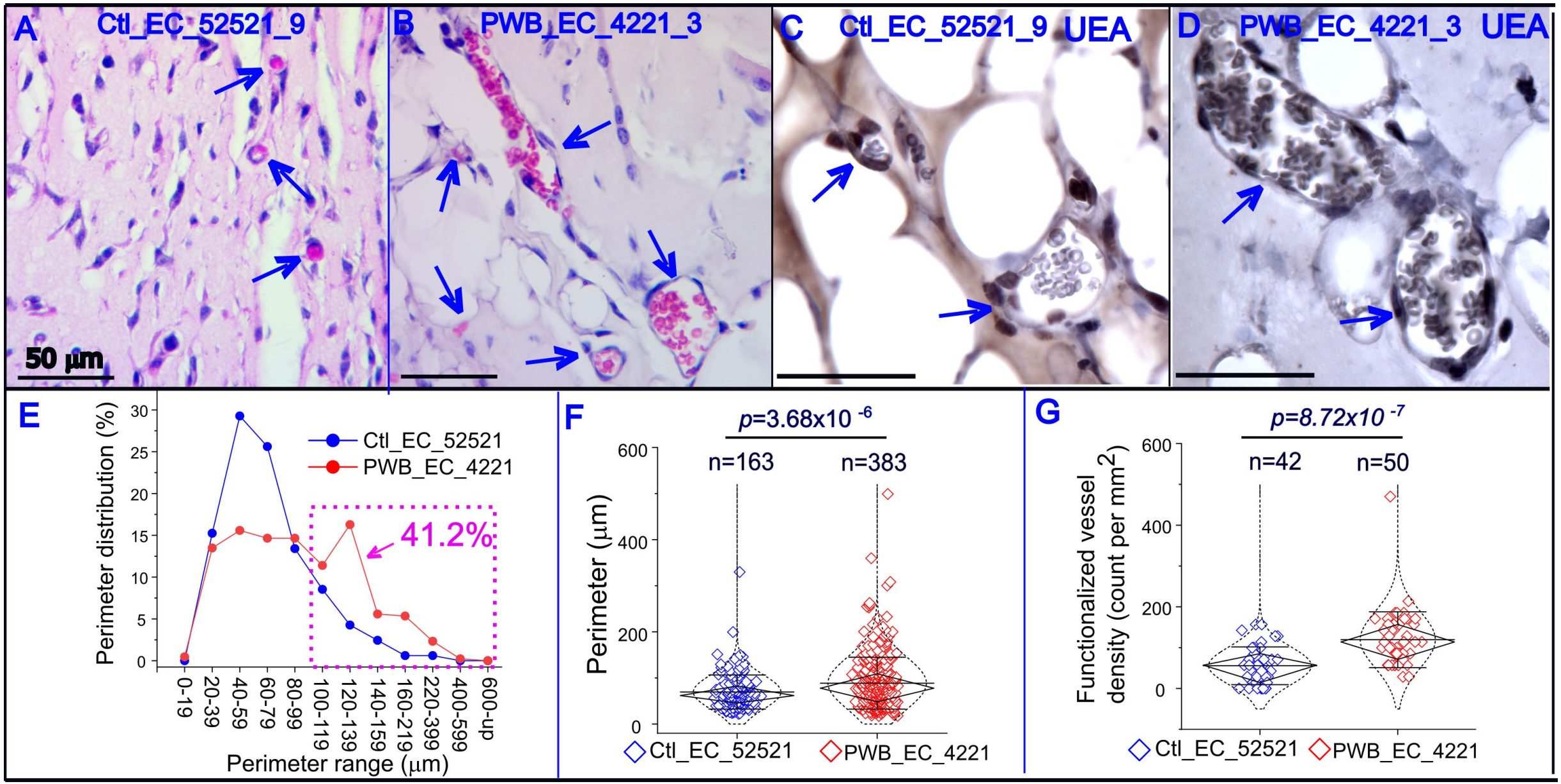
A
Ctl_EC_52521_9
50 µm
B
PWB_EC_4221_3
C
Ctl_EC_52521_9
UEA
D
PWB_EC_4221_3
UEA
E
Perimeter distribution (%)
Ctl_EC_52521
PWB_EC_4221
41.2%
0-19
20-39
40-59
60-79
80-99
100-119
120-139
140-159
160-219
220-399
400-599
600-up
Perimeter range (µm)
F
p=3.68x10 -6
n=163
n=383
Perimeter (µm)
Ctl_EC_52521
PWB_EC_4221
G
p=8.72x10 -7
n=42
n=50
Functionalized vessel density (count per mm2)
Ctl_EC_52521
PWB_EC_4221

Fig 4

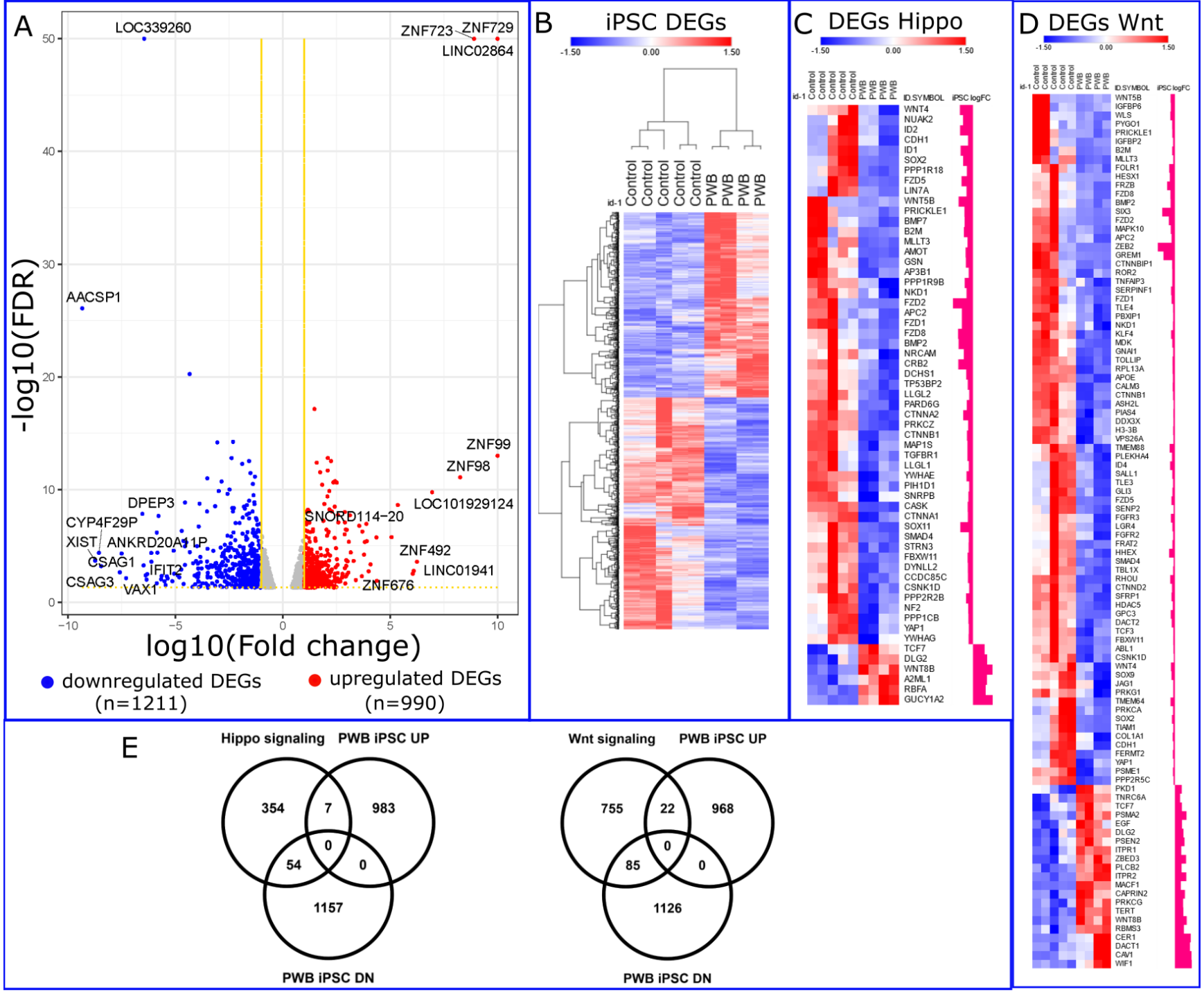
A
LOC339260
ZNF723
ZNF729
LINC02864
AACSP1
ZNF99
ZNF98
DPEP3
CYP4F29P
XIST
ANKRD20A11P
CSAG1
IFIT2
CSAG3
VAX1
SNORD114-20
LOC101929124
ZNF492
LINC01941
ZNF676
-log10(FDR)
log10(Fold change)
downregulated DEGs (n=1211)
upregulated DEGs (n=990)
B iPSC DEGs
C DEGs Hippo
D DEGs Wnt
id-1
Control
PWB
ID.SYMBOL
iPSC.logFC
E
Hippo signaling
PWB iPSC UP
354
7
983
0
54
0
1157
PWB iPSC DN
Wnt signaling
PWB iPSC UP
755
22
968
0
85
0
1126
PWB iPSC DN

Fig 5

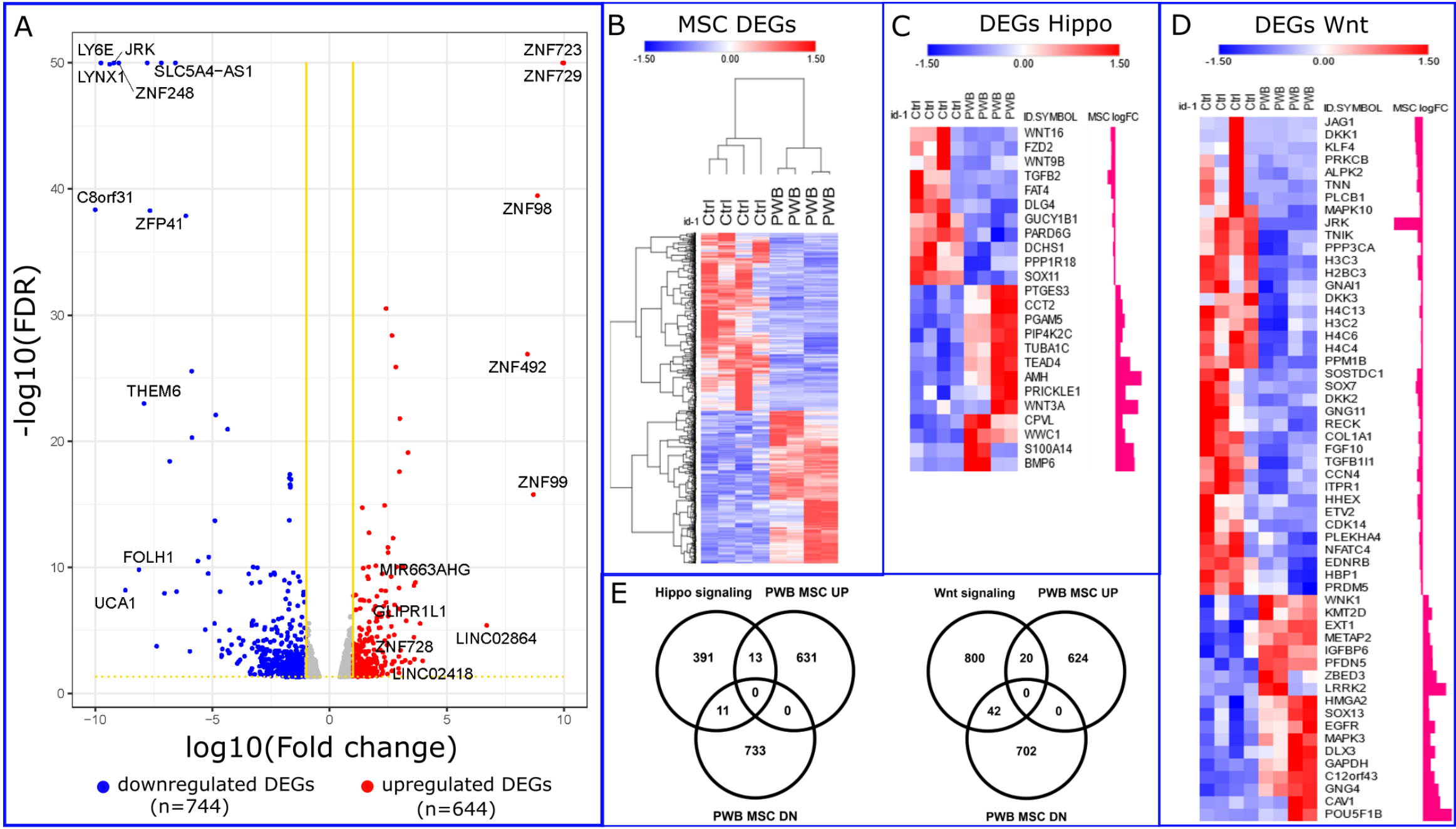
A
LY6E
JRK
LYNX1
SLC5A4-AS1
ZNF248
C8orf31
ZFP41
THEM6
FOLH1
UCA1
ZNF723
ZNF729
ZNF98
ZNF492
ZNF99
MIR663AHG
GLIPR1L1
LINC02864
ZNF728
LINC02418
-log10(FDR)
log10(Fold change)
downregulated DEGs (n=744)
upregulated DEGs (n=644)
B
MSC DEGs
-1.50
0.00
1.50
id-1
Ctrl
PWB
C
DEGs Hippo
ID.SYMBOL
MSC logFC
WNT16
FZD2
WNT9B
TGFB2
FAT4
DLG4
GUCY1B1
PARD6G
DCHS1
PPP1R18
SOX11
PTGES3
CCT2
PGAM5
PIP4K2C
TUBA1C
TEAD4
AMH
PRICKLE1
WNT3A
CPVL
WWC1
S100A14
BMP6
D
DEGs Wnt
JAG1
DKK1
KLF4
PRKCB
ALPK2
TNN
PLCB1
MAPK10
JRK
TNIK
PPP3CA
H3C3
H2BC3
GNAI1
DKK3
H4C13
H3C2
H4C6
H4C4
PPM1B
SOSTDC1
SOX7
DKK2
GNG11
RECK
COL1A1
FGF10
TGFB1I1
CCN4
ITPR1
HHEX
ETV2
CDK14
PLEKHA4
NFATC4
EDNRB
HBP1
PRDM5
WNK1
KMT2D
EXT1
METAP2
IGFBP6
PFDN5
ZBED3
LRRK2
HMGA2
SOX13
EGFR
MAPK3
DLX3
GAPDH
C12orf43
GNG4
CAV1
POU5F1B
E
Hippo signaling
PWB MSC UP
PWB MSC DN
391
13
631
0
11
0
733
Wnt signaling
PWB MSC UP
PWB MSC DN
800
20
624
0
42
0
702

Fig 6

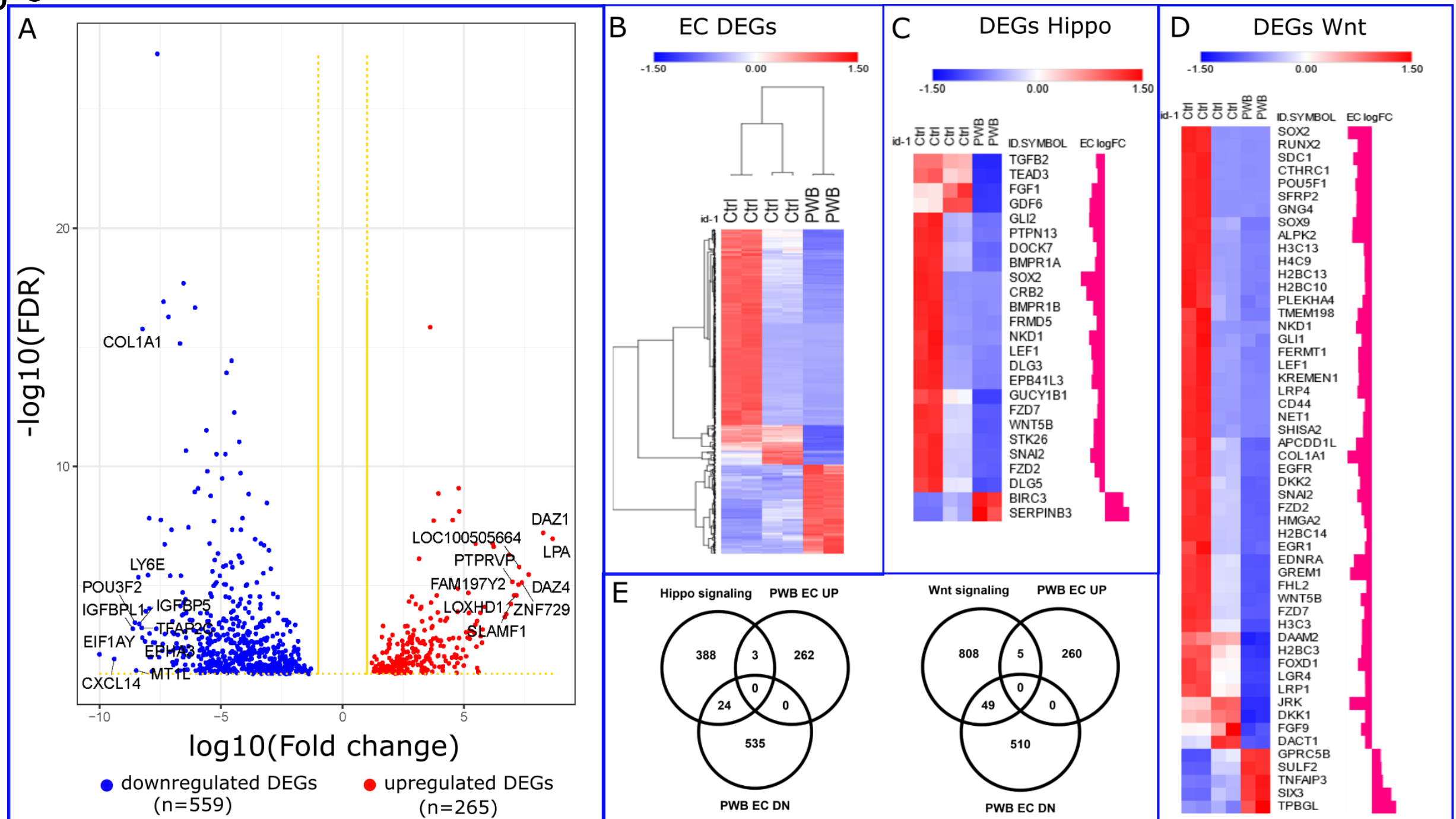
A
-log10(FDR)
log10(Fold change)
COL1A1
LY6E
POU3F2
IGFBPL1
IGFBP5
TFAP2C
EIF1AY
EPHA3
MT1L
CXCL14
DAZ1
LOC100505664
LPA
PTPRVP
FAM197Y2
DAZ4
LOXHD1
ZNF729
SLAMF1
downregulated DEGs (n=559)
upregulated DEGs (n=265)
B
EC DEGs
-1.50
0.00
1.50
id-1
Ctrl
PWB
C
DEGs Hippo
ID.SYMBOL
EC logFC
TGFB2
TEAD3
FGF1
GDF6
GLI2
PTPN13
DOCK7
BMPR1A
SOX2
CRB2
BMPR1B
FRMD5
NKD1
LEF1
DLG3
EPB41L3
GUCY1B1
FZD7
WNT5B
STK26
SNAI2
FZD2
DLG5
BIRC3
SERPINB3
D
DEGs Wnt
E
Hippo signaling
PWB EC UP
PWB EC DN
388
3
262
0
24
0
535
Wnt signaling
808
5
260
0
49
0
510

Fig 7

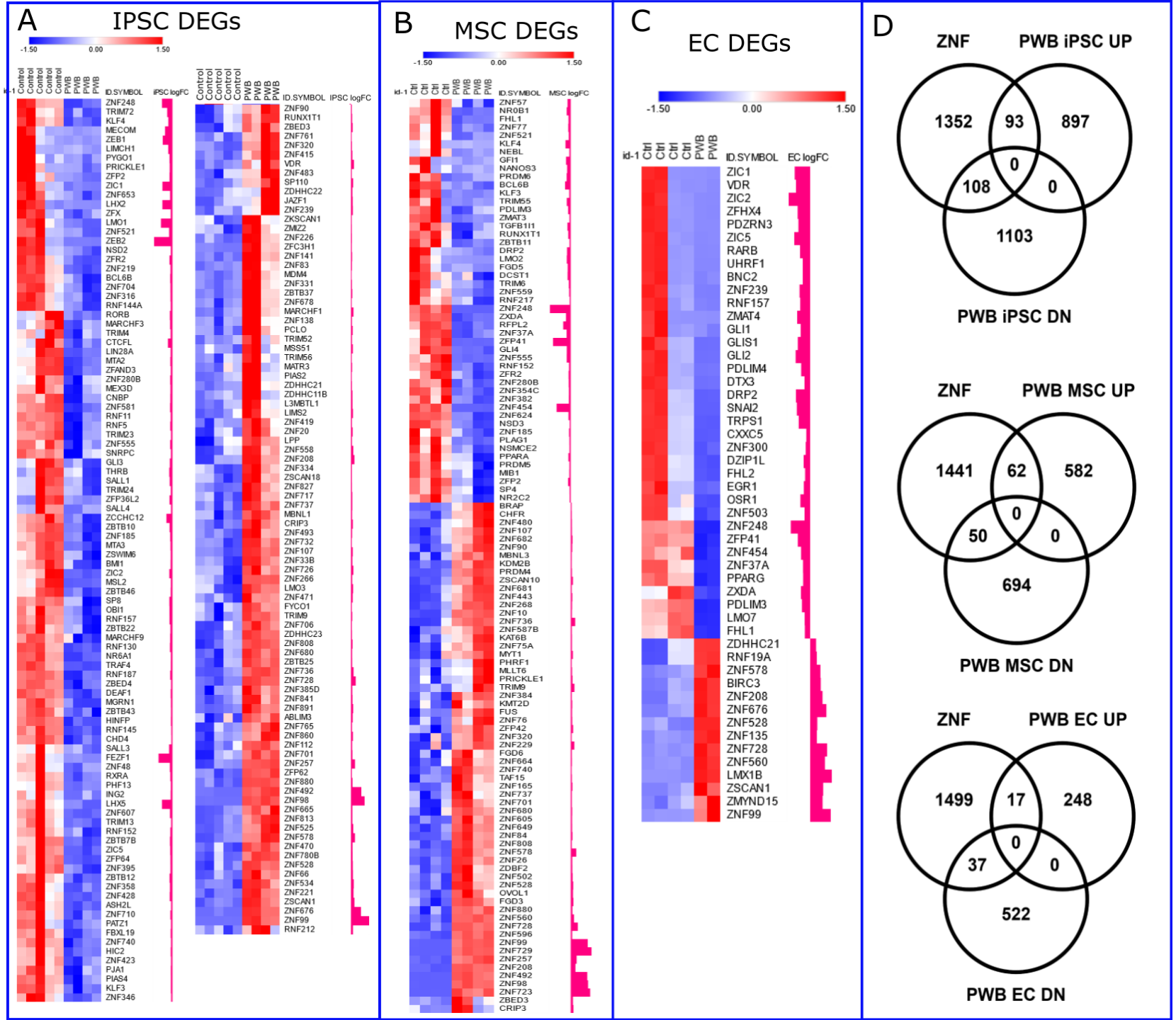
A
IPSC DEGs
-1.50
0.00
1.50
id-1
Control
PWB
ID.SYMBOL
iPSC logFC
B
MSC DEGs
MSC logFC
C
EC DEGs
EC logFC
Ctrl
D
ZNF
PWB iPSC UP
1352
93
897
0
108
0
1103
PWB iPSC DN
PWB MSC UP
1441
62
582
0
50
0
694
PWB MSC DN
PWB EC UP
1499
17
248
0
37
0
522
PWB EC DN

Fig 8

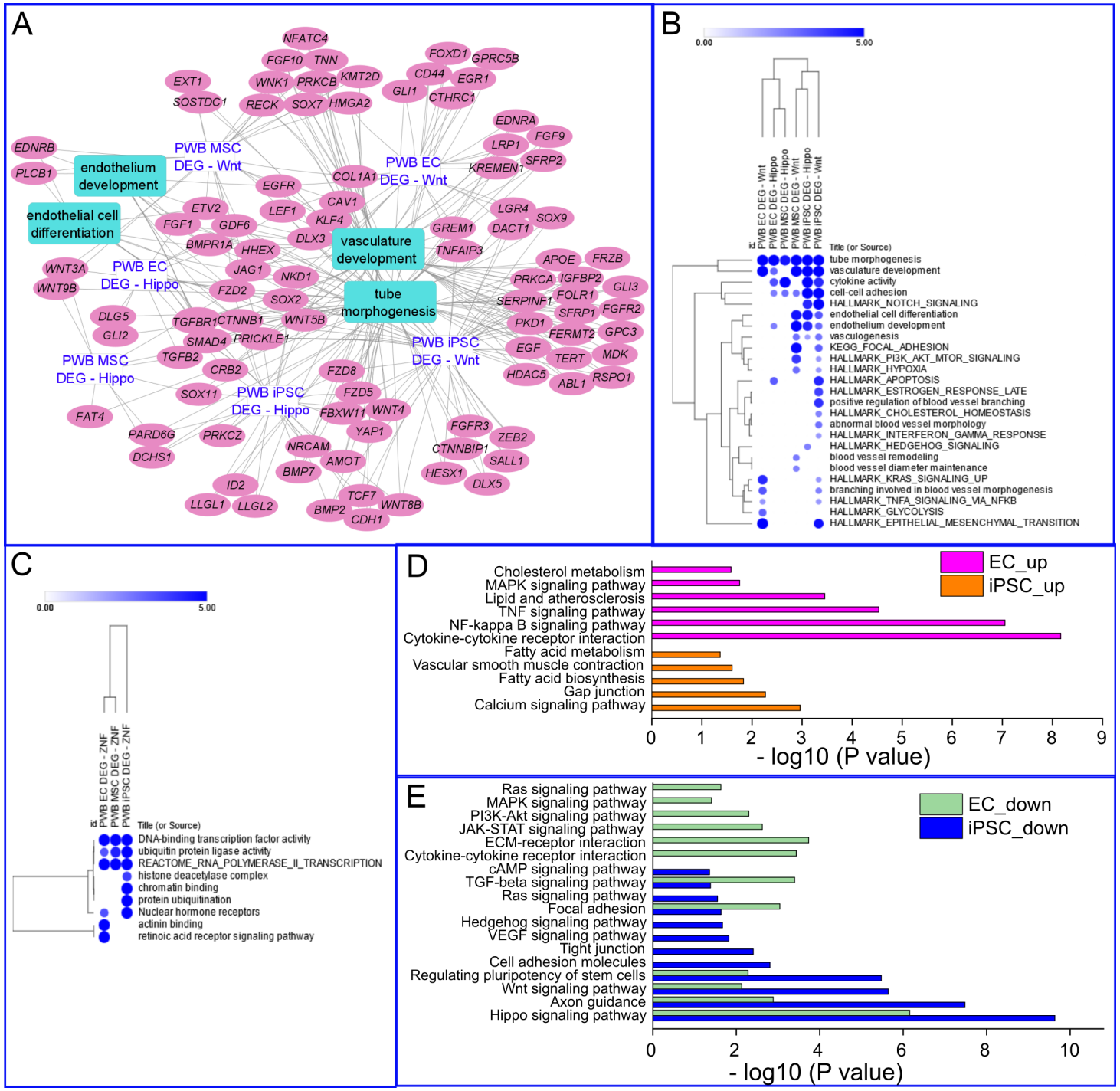
A
endothelium development
endothelial cell differentiation
vasculature development
tube morphogenesis
PWB MSC DEG - Wnt
PWB EC DEG - Wnt
PWB EC DEG - Hippo
PWB MSC DEG - Hippo
PWB iPSC DEG - Wnt
PWB iPSC DEG - Hippo
NFATC4
FGF10
TNN
FOXD1
GPRC5B
EXT1
WNK1
PRKCB
KMT2D
CD44
EGR1
SOSTDC1
RECK
SOX7
HMGA2
GLI1
CTHRC1
EDNRA
FGF9
EDNRB
LRP1
SFRP2
PLCB1
KREMEN1
COL1A1
EGFR
CAV1
ETV2
LEF1
KLF4
LGR4
SOX9
FGF1
GDF6
GREM1
DACT1
BMPR1A
HHEX
DLX3
TNFAIP3
APOE
FRZB
WNT3A
JAG1
NKD1
PRKCA
IGFBP2
GLI3
WNT9B
FZD2
SOX2
SERPINF1
FOLR1
FGFR2
DLG5
TGFBR1
CTNNB1
WNT5B
SFRP1
PKD1
GPC3
GLI2
SMAD4
PRICKLE1
FERMT2
EGF
MDK
TGFB2
TERT
CRB2
FZD8
HDAC5
RSPO1
ABL1
SOX11
FZD5
FAT4
FBXW11
WNT4
FGFR3
PARD6G
PRKCZ
YAP1
ZEB2
DCHS1
NRCAM
CTNNBIP1
SALL1
AMOT
BMP7
HESX1
ID2
DLX5
TCF7
LLGL1
LLGL2
WNT8B
BMP2
CDH1
B
0.00
5.00
id
PWB EC DEG - Wnt
PWB EC DEG - Hippo
PWB MSC DEG - Hippo
PWB MSC DEG - Wnt
PWB iPSC DEG - Hippo
PWB iPSC DEG - Wnt
Title (or Source)
tube morphogenesis
vasculature development
cytokine activity
cell-cell adhesion
HALLMARK_NOTCH_SIGNALING
endothelial cell differentiation
endothelium development
vasculogenesis
KEGG_FOCAL_ADHESION
HALLMARK_PI3K_AKT_MTOR_SIGNALING
HALLMARK_HYPOXIA
HALLMARK_APOPTOSIS
HALLMARK_ESTROGEN_RESPONSE_LATE
positive regulation of blood vessel branching
HALLMARK_CHOLESTEROL_HOMEOSTASIS
abnormal blood vessel morphology
HALLMARK_INTERFERON_GAMMA_RESPONSE
HALLMARK_HEDGEHOG_SIGNALING
blood vessel remodeling
blood vessel diameter maintenance
HALLMARK_KRAS_SIGNALING_UP
branching involved in blood vessel morphogenesis
HALLMARK_TNFA_SIGNALING_VIA_NFKB
HALLMARK_GLYCOLYSIS
HALLMARK_EPITHELIAL_MESENCHYMAL_TRANSITION
C
0.00
5.00
id
PWB EC DEG - ZNF
PWB MSC DEG - ZNF
PWB iPSC DEG - ZNF
Title (or Source)
DNA-binding transcription factor activity
ubiquitin protein ligase activity
REACTOME_RNA_POLYMERASE_II_TRANSCRIPTION
histone deacetylase complex
chromatin binding
protein ubiquitination
Nuclear hormone receptors
actinin binding
retinoic acid receptor signaling pathway
D
EC_up
iPSC_up
Cholesterol metabolism
MAPK signaling pathway
Lipid and atherosclerosis
TNF signaling pathway
NF-kappa B signaling pathway
Cytokine-cytokine receptor interaction
Fatty acid metabolism
Vascular smooth muscle contraction
Fatty acid biosynthesis
Gap junction
Calcium signaling pathway
0 1 2 3 4 5 6 7 8 9
- log10 (P value)
E
EC_down
iPSC_down
Ras signaling pathway
MAPK signaling pathway
PI3K-Akt signaling pathway
JAK-STAT signaling pathway
ECM-receptor interaction
Cytokine-cytokine receptor interaction
cAMP signaling pathway
TGF-beta signaling pathway
Ras signaling pathway
Focal adhesion
Hedgehog signaling pathway
VEGF signaling pathway
Tight junction
Cell adhesion molecules
Regulating pluripotency of stem cells
Wnt signaling pathway
Axon guidance
Hippo signaling pathway
0 2 4 6 8 10
- log10 (P value)